LIMITATIONS OF INTRABEAM SCATTERING THEORIES FOR HIGH-DENSITY BEAMS

A. Khan*[1], G. Stupakov[2], V. Smaluk[1], T. Shaftan[1]
[1]NSLS-II, BNL, Upton, NY, USA
[2]xLight Inc., Palo Alto, CA, USA

Abstract

We examine the regime of validity of classical intrabeam scattering (IBS) formalisms for ultra-low-emittance storage rings. These theories share foundational assumptions—Gaussian beam distributions, weak binary perturbations, and uncorrelated two-body encounters—that break down progressively as emittance decreases. We clarify the hierarchy among these formalisms, identifying the specific approximations that connect them and that become less accurate in the parameter range of modern machines. Using a parametric FODO lattice scan spanning two orders of magnitude in horizontal emittance, we identify quantitative boundaries where each assumption fails: below a critical emittance the IBS-to-damping ratio exceeds unity, the large-angle collision time collapses by several orders of magnitude, and the plasma response time approaches the scattering time scale.

INTRODUCTION

Intrabeam scattering is one of the key factors limiting the performance of modern high-brightness synchrotron light sources at high beam intensity [1]. The foundational theories of IBS were developed by Piwinski [2] and Bjorken and Mtingwa [3] in the 1970s and 1980s, when typical beam emittances were on the order of a few to tens of nm·rad. Since then, storage ring emittances have been reduced by up to two orders of magnitude in multi-bend achromat (MBA) lattices now being deployed at fourth-generation light sources [1], reaching the sub-nm·rad regime. The assumptions underlying the classical IBS formalisms—Gaussian beam distributions, weak binary perturbations, and uncorrelated two-body encounters—were never designed for this regime, yet they continue to be used as the primary prediction tools.

In this study, we examine where those assumptions break down. We first clarify the hierarchy among the classical formalisms, identifying the approximations that connect them. We then use a parametric FODO lattice scan to identify quantitative boundaries where each foundational assumption fails.

CLASSICAL IBS FORMALISMS AND THEIR ASSUMPTIONS

Piwinski and Bjorken-Mtingwa

The first comprehensive IBS theory was developed by Piwinski [2], who computed momentum-transfer rates from two-body Coulomb collisions using classical kinematics with the Rutherford cross section for a smooth-lattice Gaussian beam. He later extended the theory to include linear coupling and arbitrary beam sizes [4]. Bjorken and Mtingwa (B-M) independently derived IBS growth rates from relativistic quantum field theory [3], evaluating the rates through a phase-space integral at each lattice point with a cubic-polynomial denominator in the integration variable λ. Extensions with vertical dispersion and non-ultrarelativistic corrections exist for MAD-X [5], and coupled generalizations require the Lebedev-Nagaitsev-Mais-Ripken formalism [6]. Nagaitsev [7] reformulated the B-M integrals using Carlson's symmetric elliptic integrals, producing results strictly identical to B-M but roughly 20 times faster to evaluate. The same growth rates follow independently from the Landau kinetic equation [8] applied to the beam-frame velocity distribution [9]. In the ultrarelativistic limit $\gamma^2 \gg \beta_{x,y}/\epsilon_{x,y}$ the λ^3 term in the B-M denominator is negligible and the full B-M result reduces exactly to the Nagaitsev-Lebedev expressions.

Revised Bane's High-Energy Approximation

Bane's high-energy approximation [10] introduces simplifications to B-M but makes approximations some of which are only valid when dispersion is relatively small. We would like to point out that a more accurate and still relatively simple approximation can be found in Ref. [9], p. 199. This approximation is also obtained for high-energy taking into account that in practice the longitudinal temperature in the beam frame is much smaller than the transverse one. For the rate of the relative energy spread σ_δ, this approximation, after some transformations, can be written as:

$$\frac{d\sigma_\delta^2}{dt} = \frac{N r_0^2 c}{4\sqrt{2}\gamma^3 \sigma_z} \left\langle \frac{\Lambda}{\tilde{\sigma}_x \sigma_y} \tilde{\Upsilon}(\theta_x, \theta_y) \right\rangle_s , \qquad (1)$$

where N is the number of particles in the bunch, $\tilde{\sigma}_x^2 = \epsilon_x \beta_x + \sigma_\delta^2 D_x^2$,

$$\theta_x^2 = \frac{\epsilon_x}{\beta_x}\left(1 + \frac{\sigma_\delta^2}{\sigma_x^2}(\beta_x D_x' + \alpha_x D_x)^2\right), \qquad \theta_y^2 = \frac{\epsilon_y}{\beta_y}, \quad (2)$$

and

$$\tilde{\Upsilon}(x,y) = \frac{2^{1/2}}{\pi} \int_0^\infty \frac{d\lambda}{\sqrt{(1+x^2\lambda^2)(1+y^2\lambda^2)}}. \qquad (3)$$

Here Λ is the Coulomb logarithm and we use the standard notations for the lattice functions and the beam parameters. The angular brackets in Eq. (1) indicate averaging over the circumference of the ring.

* akhan1@bnl.gov

Bane's formulas can be obtained from Eqs. (1)-(3) by 1) dropping the dispersion–energy-spread cross-terms in Eq. (2) and using $\theta_x \approx \sqrt{\epsilon_x/\beta_x}$ (which may be justified if dispersion is small) and 2) using $\hat{\sigma}_x^2 = \epsilon_x\beta_x + \sigma_\delta^2\mathcal{H}\beta_x$ instead of $\tilde{\sigma}_x^2$ (which is hard to justify).

The Bane form is nonetheless the most widely used in current lattice design practice and is the formula evaluated in the parametric scan of the next section.

Shared Assumptions

All formalisms described above rest on the following foundational assumptions:

(A1) Gaussian beam distribution. The beam distribution is taken to be Gaussian in all three planes throughout the calculation

(A2) Weak perturbation. Individual momentum kicks satisfy $|\Delta p|/p \ll \sigma_\delta$, so the collision integral can be treated as a diffusion (Fokker–Planck) process.

(A3) Uncorrelated binary collisions. Successive scattering events are statistically independent; no collective correlations persist on the scattering time scale.

(A4) Perturbative equilibrium. IBS inflates the emittance only as a small correction to the radiation-damped equilibrium. The standard ansatz $\epsilon_x = \epsilon_{x0}/(1 - \tau_x/T_x)$ requires $\tau_x/T_x \ll 1$. A recent Vlasov-equation analysis shows that this ansatz is not justified when the ratio approaches or exceeds unity [11].

Experimental evidence already challenges (A1) directly. Measurements at Cornell Electron Storage Ring Test Accelerator (CESR-TA) as discussed [12] found that reconciling IBS predictions with observed beam sizes required a "tail-cut" procedure in which rare large-angle scattering events are excluded from the growth-rate calculation. The need for such a correction indicates that the beam distribution develops non-Gaussian tails that lie outside the domain of validity of the standard theory. Therefore, the proper consideration of these tails requires solving the steady-state Vlasov equation with the full collision integral, rather than computing growth rates from an assumed Gaussian.

This issue also highlights a deeper structural point. IBS and Touschek scattering are conventionally treated as separate phenomena—small-angle diffusion versus rare large-angle loss—but both originate from the same Coulomb interaction, and there is no sharp physical boundary between them. The distinction is imposed by the theoretical approximation, and its reliability depends on conditions quantified in the next section.

FODO LATTICE SCAN: QUANTITATIVE REGIME DIAGNOSTICS

Lattice Family Construction

To test assumptions (A1)–(A4) quantitatively, we construct a family of optically-scaled FODO storage rings. All members share a fixed circumference $C = 500$ m, beam energy $E = 3$ GeV, and RF system with $f_{\rm rf} = 500$ MHz (harmonic number $h = 834$). The number of identical FODO cells N_c is varied from 85 to 450. Each cell contains two dipoles with bend angle $\theta_b = \pi/N_c$; element lengths scale as $L \propto 1/N_c$ and quadrupole gradients as $K_1 \propto N_c^2$, preserving the phase advance per cell to leading order. The natural horizontal emittance consequently scales as $\epsilon_{x0} \propto 1/N_c^3$, spanning from approximately 1900 pm at $N_c = 85$ down to 13 pm at $N_c = 450$.

The rms bunch length is $\sigma_s \approx 3$ mm with momentum spread $\sigma_\delta \approx 4.51 \times 10^{-4}$ throughout the family. A fixed coupling ratio $\kappa = \epsilon_y/\epsilon_x = 0.1$ is used. The radiation damping times are $\tau_x \approx 45.3$ ms and $\tau_\delta \approx 22.7$ ms for all lattices, so all variation in the results is driven by optics and emittance changes alone. IBS growth rates are evaluated using the Bane high-energy approximation, which provides a computationally efficient formulation well suited for fast lattice parameter scans such as the FODO study.

Growth Rates and IBS-to-Damping Ratio

Table 1 collects the average optics functions, natural emittance, and IBS growth rates. Both $1/T_x$ and $1/T_p$ rise by more than three orders of magnitude across the scan.

Table 1: Equilibrium parameters and IBS growth rates

N_c	$\langle\beta_x\rangle$ [m]	$\langle\beta_y\rangle$ [m]	$\langle D_x\rangle$ [m]	ϵ_x [pm]	$1/T_x$ [s^{-1}]	$1/T_p$ [s^{-1}]
85	6.2	5.6	0.130	1727	1.1	1.8
120	4.4	4.2	0.060	614	6.3	10.1
222	2.4	2.3	0.020	97	134	215
366	1.4	1.4	0.007	22	1586	2545
450	1.2	1.1	0.001	12	4443	7127

To assess where IBS transitions from a perturbation to a dominant effect, we form the dimensionless ratios $R_x \equiv \tau_x/T_x$ and $R_p \equiv \tau_\delta/T_p$, comparing the IBS growth time directly to the radiation damping time. Results are shown in Fig. 1.

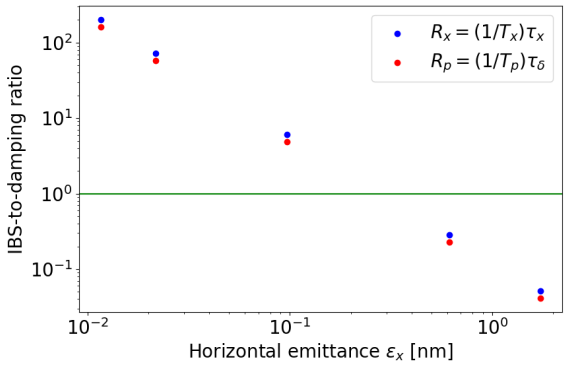

Figure 1: Dimensionless IBS-to-damping ratios $R_x = (1/T_x)\tau_x$ and $R_p = (1/T_p)\tau_\delta$ plotted versus ε_x for the FODO lattice family.

For this lattice family, R_x crosses unity in the range of a few hundred picometers. We refer to this boundary as the

critical emittance. It marks the point below which assumption (A4) fails and the perturbative ansatz loses quantitative reliability. At $N_c = 222$ ($\epsilon_x = 97$ pm), R_x already exceeds six.

Beam-Frame Diagnostics

To probe assumptions (A2) and (A3) directly, we evaluate beam-frame quantities. The transverse beam-frame temperature $T_{x0} = mc^2\gamma^2\epsilon_x/\beta_x$ characterizes the kinetic energy of random transverse motion in the beam frame. As emittance decreases, the beam becomes transversely "colder": particles move more slowly relative to each other, allowing closer Coulomb encounters before deflection. The minimum approach distance for large-angle collisions, $r_{\min} = r_e\, mc^2/T_{x0}$, therefore grows with decreasing emittance, increasing the cross section for hard scattering events.

The beam-frame density is $n = N/[(2\pi)^{3/2}\gamma\beta_x\epsilon_x\sigma_s]$, from which the large-angle collision time $\tau_{\text{coll}} = (n\,\pi r_{\min}^2\, v)^{-1}$ (with $v \sim c\sqrt{T_{x0}/mc^2}$) and the plasma frequency $\omega_p = (ne^2/\varepsilon_0 m)^{1/2}$ follow. Results are collected in Table 2.

Table 2: Beam-frame diagnostics across the FODO scan

N_c	T_{x0} [keV]	$r_{\min}$ [pm]	$\tau_{\text{coll,lab}}$ [h]	ω_p [10^9/s]
85	4.91	0.29	24.6	5.2
120	2.47	0.58	2.15	10.4
222	0.72	2.00	0.029	35.8
366	0.27	5.41	0.0012	84.2
450	0.18	8.22	0.0002	154

Interpretation

Three trends in Table 2 are significant for assessing the foundational assumptions. First, $r_{\min}$ grows by a factor of nearly 30 across the scan, reflecting the transverse cooling of the beam. The individual scattering events become harder as the beam gets colder.

Second, $\tau_{\text{coll,lab}}$ collapses by approximately five orders of magnitude, from hours to sub-millisecond time scales. At the low-emittance end, hard scattering events occur on time scales comparable to or shorter than the radiation damping time. This directly challenges assumption (A2): when large-angle kicks become frequent, the diffusion approximation underlying the Fokker–Planck treatment of the collision integral is no longer well justified. It also undermines the conventional separation between IBS and Touschek scattering, since the "rare" large-angle events are no longer rare.

Third, ω_p increases by a factor of ~ 30 while $\tau_{\text{coll,lab}}$ simultaneously collapses. As the relevant scattering time scale approaches the collective response time set by the plasma frequency, the assumption of uncorrelated binary encounters (A3) comes under pressure. A precise quantitative threshold for the failure of (A3) has not been established in the present work. This trend is flagged as requiring further investigation.

Taken together, these diagnostics show that for this FODO family the assumptions underlying classical IBS theory begin to fail in the range $\epsilon_x \approx 100$–600 pm and become increasingly unreliable below 100 pm.

DISCUSSION

Complications in MBA Lattices

The FODO scan isolates the effect of emittance reduction in a uniform lattice. In real MBA lattices the contribution to horizontal emittance growth via IBS is strongly localized in the high-dispersion arc cells, since the horizontal growth rate is weighted by the dispersion invariant $\mathcal{H}$, which vanishes in dispersion-free straights. Ring-averaged approximations suppress this localization and can misestimate the dominant contribution

These considerations suggest that, for MBA lattices, IBS should be evaluated with local lattice information and, ultimately, within a framework that can treat non-Gaussian distributions self-consistently.

A further complication is the widespread use of higher-harmonic cavities (HHCs) for bunch lengthening and lifetime improvement in low-emittance rings [13, 14]. HHCs flatten the RF potential and can generate longitudinal distributions that deviate significantly from a Gaussian, especially in multi-harmonic configurations and near optimal bunch-lengthening conditions. Studies for ultra low-emittance rings show that multi-higher-harmonic systems can substantially modify the bunch shape and lengthening factor, reinforcing the need for IBS models that go beyond the Gaussian assumption.

Toward a Self-Consistent Framework

The analysis above identifies where the classical formalisms break down but does not yet provide a replacement. A path toward a self-consistent treatment has been developed [11]: starting from the Landau collision integral expressed in laboratory-frame coordinates, a collision term St_{IBS} is derived as a function of the action variable J_x without assuming a Gaussian distribution. The steady-state beam distribution is then obtained by solving the Vlasov equation $\text{St}_{\text{ISR}}\, f + \text{St}_{\text{IBS}}\, f = 0$, where St_{ISR} accounts for synchrotron radiation damping and quantum diffusion. This equation reduces to the standard exponential distribution $f \propto e^{-J/J_c}$ when IBS is absent, and predicts deviations from this form—including non-Gaussian tails—when IBS is strong. Full results from this approach will be reported separately.

ACKNOWLEDGMENT

This work was supported by the U.S. Department of Energy, Office of Science, Early Career Research Program under Award No. DE-SCL0000016.

REFERENCES

[1] V. Smaluk, T. Shaftan, and D. Hidas, "Ultimate brightness of a medium-energy synchrotron light source at operational beam intensity", *J. Synchrotron Radiat.*, vol. 32, no. 3, 2025. doi:10.1107/S1600577525002723

[2] A. Piwinski, "Intra-beam-scattering", in *Proc. 9th International Conference on High-energy Accelerators*, Stanford, CA, USA, May 1974. doi:10.5170/CERN-1992-001.226

[3] J. D. Bjorken and S. K. Mtingwa, "Intrabeam scattering", *Part. Accel.*, vol. 13, no. FERMILAB-PUB-82-47-THY, pp. 115–143, 1982.

[4] A. Piwinski, "Intrabeam scattering in presence of linear coupling", DESY, Hamburg, Germany, Rep. DESY-90-113, 1990.

[5] F. Antoniou and F. Zimmermann, "Revision of Intrabeam Scattering with Non-Ultrarelativistic Corrections and Vertical Dispersion for MAD-X", CERN, Geneva, Switzerland, Rep. CERN-ATS-2012-066, 2012.

[6] V. Lebedev and S. Nagaitsev, "Multiple intrabeam scattering in X-Y coupled focusing systems", *arXiv preprint*, 2018. doi:10.48550/arXiv.1812.09275

[7] S. Nagaitsev, "Intrabeam scattering formulas for fast numerical evaluation", *Phys. Rev Spec. Top. Accel. Beams*, vol. 8, no. 6, p. 064403, 2005. doi:10.1103/PhysRevSTAB.8.064403

[8] L. D. Landau, "The transport equation in the case of coulomb interactions", *Collected Papers of LD Landau*, pp. 163–170, 1936. doi:10.1016/B978-0-08-010586-4.50029-8

[9] V. Shiltsev and V. Lebedev, *Accelerator Physics and Tevatron Collider*. Springer, 2014.

[10] K. L. F. Bane, "A simplified model of intrabeam scattering", 2002. doi:10.48550/arXiv.physics/0206002

[11] G. Stupakov, "Collision Integral in the Lab Frame", To be published.

[12] M. P. Ehrlichman *et al.*, "Intrabeam scattering studies at the Cornell Electron Storage Ring Test Accelerator", *Phys. Rev. Spec. Top. Accel. Beams*, vol. 16, no. 10, p. 104401, 2013. doi:10.1103/PhysRevSTAB.16.104401

[13] A. Khan, G. Bassi, and V. Smaluk, "Bunch lengthening induced by a combination of higher-harmonic cavities of different order in low-emittance rings", in *Proc. IPAC'24*, pp. 2952–2955, May 2024. doi:10.18429/JACoW-IPAC2024-THBD2

[14] A. Khan, G. Bassi, and V. Smaluk, "Study of the combined effect of intrabeam scattering and impedance in a low-emittance ring", in *Proc. IPAC'23*, Venice, Italy, pp. 3436–3438, May 2023. doi:10.18429/JACoW-IPAC2023-WEPL141